Macromolecules
ARTICLE

Macromolecules **2010**, *43*, 4253–4260 **4253**
DOI: 10.1021/ma902646t

Reversible Morphology Control in Block Copolymer Films via Solvent Vapor Processing: An in Situ GISAXS Study

Marvin Y. Paik,[†] Joan K. Bosworth,[†,§] Detlef-M. Smilges,[‡] Evan L. Schwartz,[†] Xavier Andre,[†,⊥] and Christopher K. Ober*[,†]

[†]*Department of Materials Science and Engineering, Cornell University, Ithaca, New York 14850,* [‡]*Cornell High Energy Synchrotron Source, Cornell University, Ithaca, New York 14853,* [§]*Hitachi Global Storage Technologies, San Jose, California 95135, and* [⊥]*Agfa Graphics NV, Septestraat 27, B-2640 Mortsel, Belgium*

Received December 1, 2009; Revised Manuscript Received March 28, 2010

ABSTRACT: The real time changes occurring within films of cylinder-forming poly(α-methylstyrene-*block*-4-hydroxystyrene) (PαMS-*b*-PHOST) were monitored as they were swollen in tetrahydrofuran (THF) and acetone solvent vapors. In situ information was obtained by combining grazing incidence small-angle X-ray scattering (GISAXS) with film thickness monitoring of the solvent vapor swollen films. We show that for self-assembly to occur the polymer thin film must surpass a swollen thickness ratio of 212% of its original thickness when swollen in THF vapors and a ratio of 268% for acetone vapor annealing. As the polymer becomes plasticized by solvent vapor uptake, the polymer chains must become sufficiently mobile to self-assemble, or reorganize, at room temperature. Using vapors of a solvent selective to one of the blocks, in our case PHOST-selective acetone, an order−order transition occurred driven by the shift in volume fraction. The BCC spherical phase assumed in the highly swollen state can be quenched by rapid drying. Upon treatment with vapor of a nonselective solvent, THF, the film maintained the cylindrical morphology suggested by its dry-state volume fraction. In situ studies indicate that self-assembly occurs spontaneously upon attaining the threshold swelling ratios.

Introduction

With the growing need for controlled fabrication of structures at the nanoscale, the self-assembly of block copolymers has garnered much attention.[1−5] Block copolymers are an attractive alternative to advanced lithographic techniques due to their ability to form a variety of well-defined morphologies with length scales ranging from 10 to 100 nm. Not only do the length scales achievable make block copolymers relevant to many nanotechnology applications, but also their chemical structure may be tailored for desired functionality. Thus, self-assembled block copolymers have found uses in microelectronics,[6] storage devices,[5] solar cells,[3] molecular sieves,[7,8] low-*k* dielectrics,[9] and organic semiconductor applications,[10,11] among others.

However, many challenges remain in controlling the ordering of the self-assembled morphologies of block copolymers. Attaining a desired morphology can be difficult as the two blocks must be immiscible for phase separation to occur, and the volume fraction ratio must lie within an appropriate region within the phase diagram.[12,13] For example, achieving a gyroidal morphology is exceptionally challenging as there is a narrow range of parameters which lead to this regime.[14] Thus, through synthesis alone, morphology control can be difficult to accomplish, and the ability to tune the morphology is attractive. Similarly, ordering can be a complicated issue as well. In certain cases, long-range ordering is difficult to achieve, as thermal annealing cannot be used with block copolymers possessing a lower thermal degradation temperature than glass transition temperature for one or both of the blocks.

The use of solvent annealing, rather than thermal annealing, to induce long-range ordering in block copolymer thin films has received recent attention,[4,5,15−17] as it not only induces orientation and ordering, but the self-assembled morphology may be reversibly tuned as well. The swelling of both blocks provides sufficient mobility for the chains to rearrange and to allow one block to preferentially wet the substrate surface.[18] If the chosen solvent displays selectivity to one of the blocks, the resulting volume change in the swollen state may lead to an order−order transition from the bulk morphology. The newly attained phase may then be kinetically trapped upon fast evaporation of the solvent.[4,19]

The pathway by which the block copolymer undergoes an order−order transition from one morphology to another during the solvent annealing process has not been fully explored. Initial studies of selective solvent vapor annealing report that the transition from cylinders to spheres occurs due to selective interactions between the solvent vapors and the individual blocks, causing one block to isolate itself resulting in the formation of spherical micelles.[19] Another study reports a monolayer of spherical micelles of poly(styrene)-*b*-poly(4-vinylpyridine) (PS-*b*-P4VP) annealed in THF to control the fusion and fission of the micelles in order to alter the morphology and improve the ordering of the self-assembled structures.[20]

We have previously reported the use of solvent annealing to induce long-range ordering in thin films of poly(α-methylstyrene)-*block*-poly(4-hydroxystyrene), or PαMS-*b*-PHOST.[4,21] Annealing in tetrahydrofuran (THF) and acetone vapors not only enhances ordering but also controls the morphology in the swollen and dried films: the nonselective THF vapor leads to a cylindrical morphology with parallel orientation, while PHOST-selective acetone leads to a spherical morphology which can be kinetically trapped upon solvent evaporation.[4] Previously, we have demonstrated that films of PαMS-*b*-PHOST may be reversibly tuned by

*To whom correspondence should be addressed.

Published on Web 04/16/2010

Scheme 1. Experimental Setup of the in Situ Solvent Annealing GISAXS Study

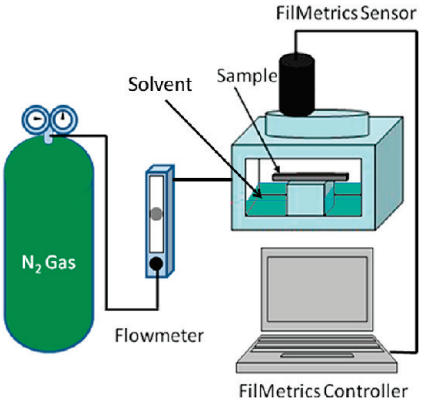

choice of annealing solvent with alternating solvent anneal sessions with THF and acetone.[4,21] In this paper, detailed insight into the mechanism of morphology formation and ordering of the self-assembled domains in solvent vapor through the use of in situ grazing incidence small-angle X-ray scattering (GISAXS) is provided.[22−26] Using GISAXS to probe the film interior during the solvent annealing process in combination with using a film thickness monitor,[26,27] a correlation between swelling ratio, solvent, and annealing time can be made. Here we show that sufficient chain mobility must be available to the polymer, and the appropriate volume fraction ratio must be attained in order for ordering and morphology change to occur during solvent treatment.

Experimental Section

Polymer Synthesis. Poly(α-methylstyrene)-*block*-poly(*tert*-butoxystyrene) (PαMS-*b*-PtBuOS) was synthesized via sequential anionic polymerization; PαMS-*b*-PHOST is formed by subsequent deprotection, as described elsewhere in the literature.[4,8,28]

Sample Preparation and Annealing. PαMS-*b*-PHOST was dissolved in propylene glycol monomethyl ether acetate (PGMEA, Aldrich) to make a 5% (w/v) solution. Thin films were prepared by spin-coating the solution at 2000 rpm onto silicon wafers. The wafers were then cut to 20 mm × 20 mm pieces to prepare samples of the appropriate dimension for in situ studies. Solvents (either THF or acetone) were injected into a small chamber, and a controlled nitrogen counterflow determined the degree of swelling (Scheme 1).[26] The flow rates of the nitrogen were controlled using a Cole-Parmer aluminum flowmeter with a high-resolution valve (143 sccm maximum flow for nitrogen). Film thickness was monitored using a Filmetrics F20 spectroscopic reflectometer. Rapid drying of the film is achieved by opening the annealing chamber, which results in a rapid (less than 1 s) evaporation of the solvent, as observed visually by a change in optical appearance of the film.

Characterization. Synthesized polymer molecular weights were measured using gel permeation chromatography (GPC). Four Waters Styragel HT columns operating at 40 °C and Waters 490 ultraviolet (254 nm wavelength) and Waters 410 refractive index detectors were used to take the measurements. The PαMS block was found to have number-average molecular weight (M_n) 7 kg/mol; the PαMS-*b*-PtBuOS was found to be 30.5 kg/mol, corresponding to a PHOST block M_n of 16 kg/mol after deprotection. Thus, we refer to this PαMS-*b*-PHOST polymer as 7K/16K. Complete deprotection is confirmed using FTIR. Film topology and surface morphology were characterized using a Veeco Dimension 3100 atomic force microscope in tapping mode.

GISAXS experiments were conducted at the Cornell High Energy Synchrotron Source (CHESS) at station G1, with initial results collected at D1 station. G1 station is provided with a high flux X-ray beam (typically 10^{13} photons/(s mm^2)) from a 50-pole wiggler in combination with a multilayer monochromator (2% bandwidth) and harmonics rejection mirrors. A 2D Quantum 1 CCD detector was used to capture the scattered images at a beam energy of 10 keV. All images were taken at an incident angle (α_i) of 0.16°, which is slightly higher than the critical angle (α_{cp}) of the polymer film. GISAXS images were taken at periodic increments of time to probe any changes occurring within the film. Because the beam was found to cross-link the film after an exposure of several seconds, thus locking the morphology in the exposed spot, the film was moved slightly through the beam for each new exposure.[22]

The sample was housed in a custom-made vapor cell with an integrated film thickness monitor[26] that could be mounted on the sample goniometer (Scheme 1). The cell has inlets for liquid solvent as well as for inert gas flow, which was used to keep the solvent vapor concentration at intermediate values compared to the equilibrium vapor pressure. The in situ film thickness monitor is based on an optical spectroscopic reflectometer (Filmetrics F20). The spot on the film probed by the light beam of the instrument was not exposed to X-rays.

Results and Discussion

In this work we probe how the reorganization of the self-assembled domains occurs via solvent vapor annealing as well as the mechanism of reorganization using in situ real time GISAXS experiments. Annealing of as-spun films in THF and acetone vapors as well as the reversible control of the morphology by alternating annealing the films from one solvent to the next were studied.

PαMS-*b*-PHOST with similar PαMS volume fraction, though larger molecular weight, directly spin-coated from PGMEA was previously found to form perpendicular cylinders, though without long-range hexagonal packing.[4,8] GISAXS and AFM confirm the same behavior for the 7K/16K polymer used here (Figure 1). The Bragg rods indicate a perpendicular cylinder morphology of the PαMS minor phase formed upon evaporation of the spinning solvent (Figure 1a). The presence of weak first-order peaks suggests that while the cylinders are all oriented perpendicular to the sample surface, there is only short-range ordering laterally. The AFM image of the as-spun surface, as seen in Figure 1b, is in agreement with the GISAXS interpretation. The lighter dots observed in the AFM image are consistent with the tops of perpendicular PαMS cylinders, and the lack of long-range hexagonal packing of these dots is consistent with the short-range order found in the GISAXS results.

Solvent annealing films of the 7K/16K PαMS-*b*-PHOST films used here in THF and acetone leads to the same behavior reported previously for similar molecular weights.[4,21] Similar to our previous study, ex-situ solvent annealing experiments with THF leads to parallel cylinder formation, while annealing in acetone leads to a face-centered orthorhombic (FCO) spherical morphology kinetically trapped in the film after rapid drying. We interpret the FCO structure to be the result of uniaxial shrinkage of the equilibrium BCC spherical morphology in swollen films upon drying.[4]

Anneal in THF. PαMS-*b*-PHOST films with a thickness far larger than the block period were used in order to be able to distinguish spherical morphologies from perpendicular cylindrical morphologies via GISAXS; here, the periodicity of the block copolymer is 18.8 nm (by AFM) and the film thickness 136 nm (film thickness monitor). THF is a good solvent for both PαMS and PHOST, and thus we expected the blocks to swell nonselectively and the cylindrical morphology to be maintained.[29]

The solvent annealing apparatus is shown in Scheme 1.[26] Solvent is injected into the chamber through a Teflon

capillary tube, and the vapor swells the film. A nitrogen gas counterflow controlled by a flowmeter moderates the solvent vapor concentration in the chamber and provides a very precise method of controlling the degree of swelling in the film. The film thickness was measured in situ with a spectroscopic reflectometer and thus facilitates a direct correlation of GISAXS images with the degree of swelling.

From previous ex situ observations of PαMS-*b*-PHOST swollen in THF, reordering is understood to occur due to the increased mobility the solvent vapor imparts onto the individual polymer chains.[4] In order to better understand the nonselective solvent annealing mechanism, the films were swollen and held at several thicknesses before rapid drying of the film in air.

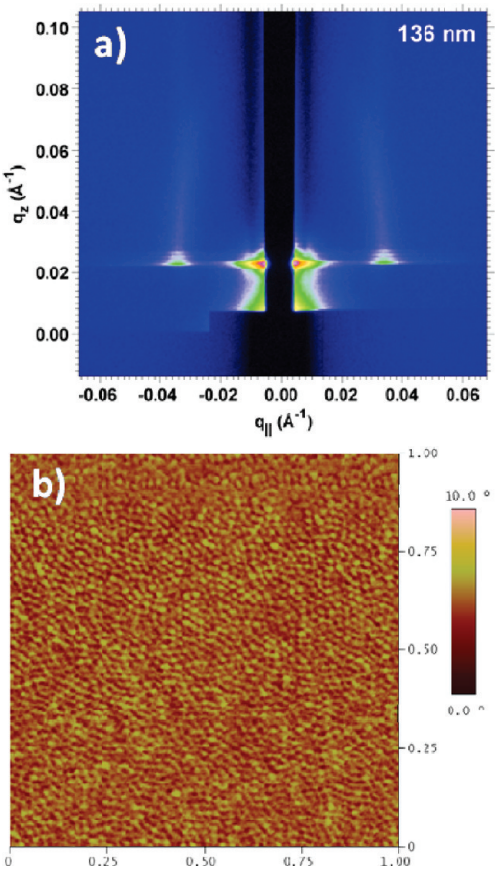

Figure 1. A film of PαMS-*b*-PHOST spin-coated from PGMEA. (a) The GISAXS profile of the as-spun block copolymer film. The Bragg rods suggests a perpendicular cylindrical morphology; however, the absence of additional ordered peaks indicates short-range ordering of the cylinders. (b) The corresponding AFM phase image confirms the morphology. The contrast scale for this image is 10°.

In the initial experiment, the PαMS-*b*-PHOST film was swollen to 214 nm (157% of the original thickness) and held for 20 min before drying the film to its original thickness. Within 8 min, the film thickness quickly increased to 174 nm, during which time the Bragg rods disappeared, leaving a featureless scattering image, seen in Figure 2a. The morphology present prior to annealing was disrupted upon the rapid swelling of the film, and no further peaks appeared during the remaining time as the thickness rose to 214 nm. Upon drying, the Bragg rods returned, but the overall intensity of those peaks had diminished significantly. While the film swelled to over 150% of its original thickness, there was apparently insufficient plasticization to induce any reordering of the self-assembled domains. The block copolymer film appears to have simply swelled and deswelled, maintaining its previous cylindrical morphology and with perpendicular orientation, albeit with slightly less order, as suggested by slightly weaker scattering in the dried film.

The initial perpendicular orientation may be the result of solvent concentration gradients, as reported by Kim and Libera for fast evaporation during spin-coating.[30] While this metastable structure has some stability with regard to gentle vapor processing, the perpendicular morphology is never obtained again after extended solvent processing in acetone and THF, as we will describe in the following.

To impart sufficient mobility to the chains for reorganization, a second film was swollen further to 297 nm (218% swelling) and held for 20 min. Like before, the Bragg rod intensity dropped within seconds upon swelling and completely disappeared after 16 min of the initial solvent injection, at a thickness of 216 nm (Figure 3a). However, upon reaching a thickness of 272 nm (200%), peaks reappeared in the same position as the as-spun film along the Yoneda peak, indicating that the initial perpendicular cylinder structure still exists but had simply been obscured by the rapid swelling (Figure 3b). As the film swells further (288 nm, 212%) a new set of peaks appear in a different position, one on the Yoneda peak and one above the Yoneda peak (Figure 3c), and the new peaks grow stronger while the initial peaks fade and disappear (Figure 3d). Upon solvent evaporation, secondary peaks appear, indicating parallel cylinder morphology (Figure 3e). The Bragg peaks in the dried films are again significantly shifted and elongated along q_z, both effects indicating an anisotropic shrinkage due to the evaporation of the film.

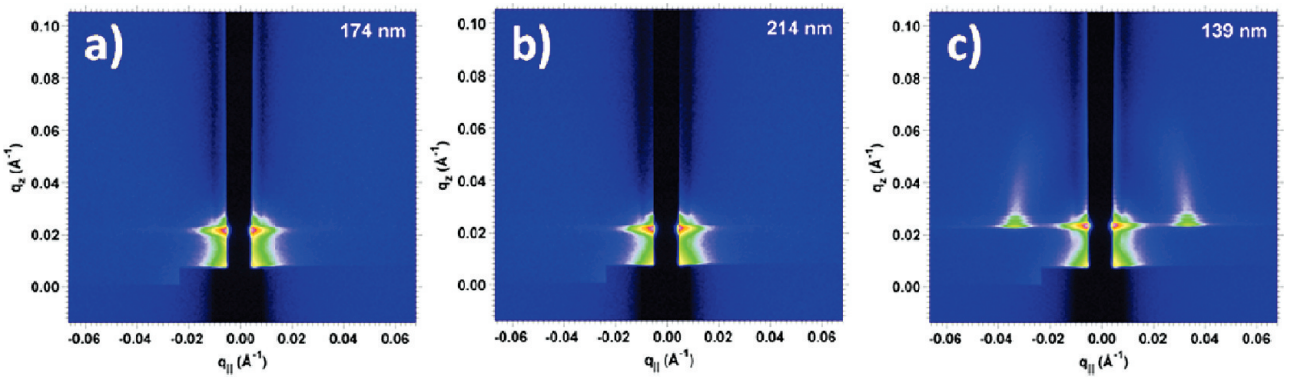

Figure 2. In situ swelling of the block copolymer film with THF vapor as seen with GISAXS. (a) The first-order peak disappears within 8 min of initial swelling, suggesting the short-range ordering that existed prior to annealing was disrupted during the rapid swelling of the film, and (b) no further peaks form even after 20 min with a gradual increase in swelling. (c) Upon rapid drying of the film, the peaks returns to a standing cylinder morphology, similar to the as-spun film. This behavior indicates that the swelling was insufficient for a change in morphology or orientation.

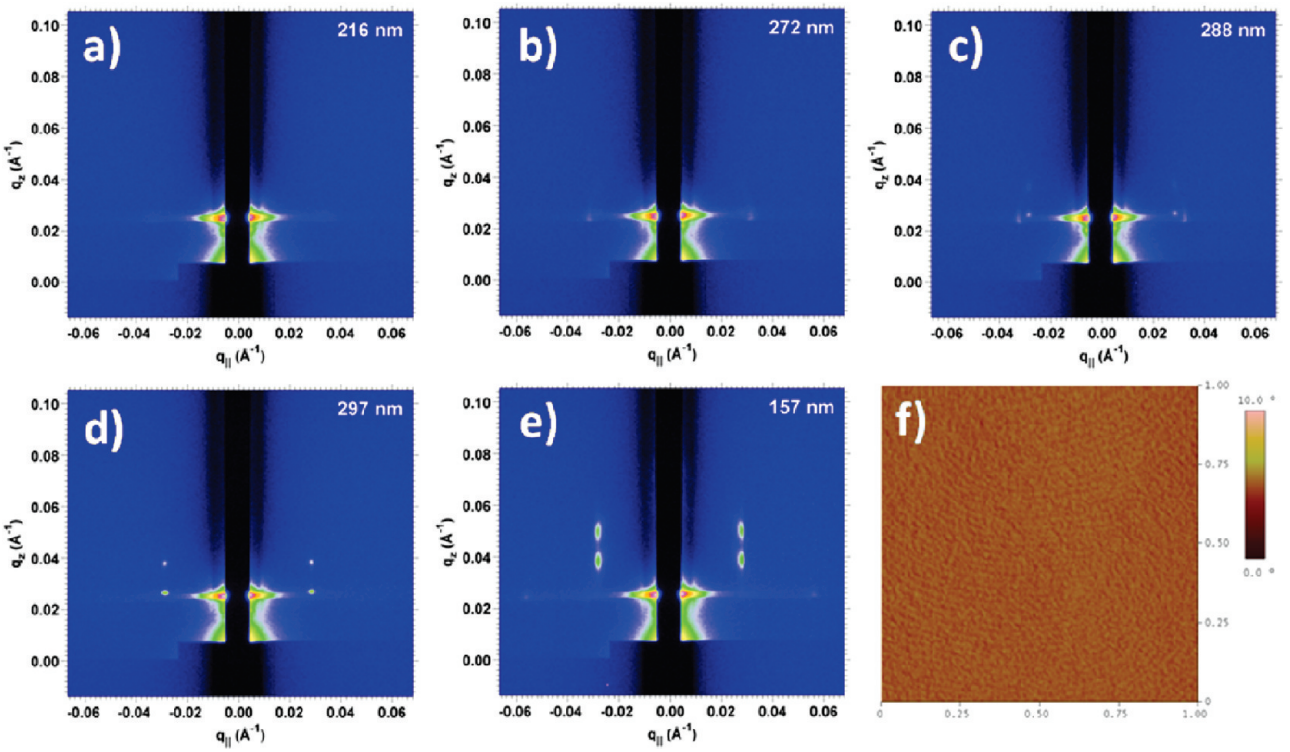

Figure 3. In situ swelling of the block copolymer thin film with THF vapor to a larger swelling ratio. (a) 18 min after beginning controlled swelling, the swelling in the film results in a disappearance of Bragg rods, indicating a disordered film. (b) As the swelling reaches 200%, peaks form on the Yoneda band in a similar position as the Bragg rods in the as-spun film. (c) Upon further swelling, a new set of peaks form, both on the Yoneda and above the Yoneda, while the original peak begins to fade. (d) The newly formed peaks become more intense, while the first peak has fully faded, indicating fully formed morphology with a distinct parallel orientation. (e) Quickly drying the film trapped in the swelled morphology and orientation, with the dried GISAXS pattern indicating the formation of parallel cylinders with shrinkage perpendicular to the substrate. (f) AFM phase image after THF solvent vapor annealing. A change from perpendicular cylinders to parallel cylinders can be seen.

The preferential attraction of one of the blocks to the substrate, or a large difference in surface tension favoring alignment of the lower surface energy block at the air interface, has been known to drive parallel orientation in block copolymer thin film morphologies.[31,32] In this case, the reappearance of the initial peak followed by its disappearance and the appearance of new peaks gives insight into the mechanism of morphology reorientation in the swollen film from perpendicular to parallel cylinders. The initial peaks corresponding to perpendicular cylinders faded, while the new peaks corresponding to parallel cylinders appeared independently and became more intense. This suggests the possibility that the perpendicular cylinders coalesced with nearby perpendicular cylinders to form new parallel cylinders. The absence of an intermediate ring structure between the first peaks and the second peaks indicates that the initial perpendicular cylinders did not simply tilt over to become parallel cylinders.

Upon evaporation of the solvent, the initial Bragg rods did not reappear, while peaks indicating cylinders oriented parallel to the surface remained. The double peak seen in Figure 3e can be attributed to the scattering of the direct beam and the reflected beam for $\alpha_i > \alpha_{cp}$: the peak in scattering intensity thus appears as a doublet and can be modeled within the framework of the distorted-wave Born approximation (DWBA).[33,34] By swelling the films to 218% of the original thickness, the swollen polymer was sufficiently plasticized for self-reorganization to occur. The selective attraction of blocks to the air and substrate interfaces is expected to induce parallel orientation of cylinders, as observed here.[35]

An interesting thing to note is that the peak positions of the dried annealed film suggest a close to hexagonally packed cylinder morphology, consistent with scattering from parallel cylinders as seen in the literature.[36] However, the q_z positions of the elevated peaks do not lie at the exact position where scattering from a hexagonally packed lattice would appear. The theoretical positions of the peaks should lie at q_z = 0.0296 and 0.0385 Å, but the actual position is q_z = 0.0382 and 0.0498 Å. The discrepancy can be attributed to a uniaxial contraction in the fast drying the film.[4] In the swollen state, the film is expected to be ordered with parallel hexagonally packed cylinders, but upon drying of the film the cylinders become compressed in the direction normal to the film surface. This compression causes the elevated peaks to shift to a slightly higher q_z positions than what is expected for a perfect hexagonal lattice. After taking into account a 42% shrinkage along the substrate normal, the theoretical and experimental q_z positions appear to match well with the theoretical q_z = 0.0389 and 0.0493 Å.

Figure 3f shows the morphology of the film after annealing in THF vapor; the fingerprint pattern present in the AFM phase image confirms the change from perpendicular to parallel cylinders. The nearest-neighbor spacing of the cylinders in the AFM image was found to be 23.3 nm, and this spacing is in good agreement with the modeled positions of the GISAXS peaks. Using a compressed hexagonally packed lattice model, the nearest-neighbor spacing was found to be 22.5 nm. Comparisons between the nearest-neighbor distances of the self-assembled structures obtained from AFM and GISAXS are shown in Table 1.

Anneal in Acetone. Acetone, while a solvent for both PαMS and PHOST, displays a preference for the PHOST majority component, and annealing in this solvent causes an order−order phase transition from a cylindrical morphology

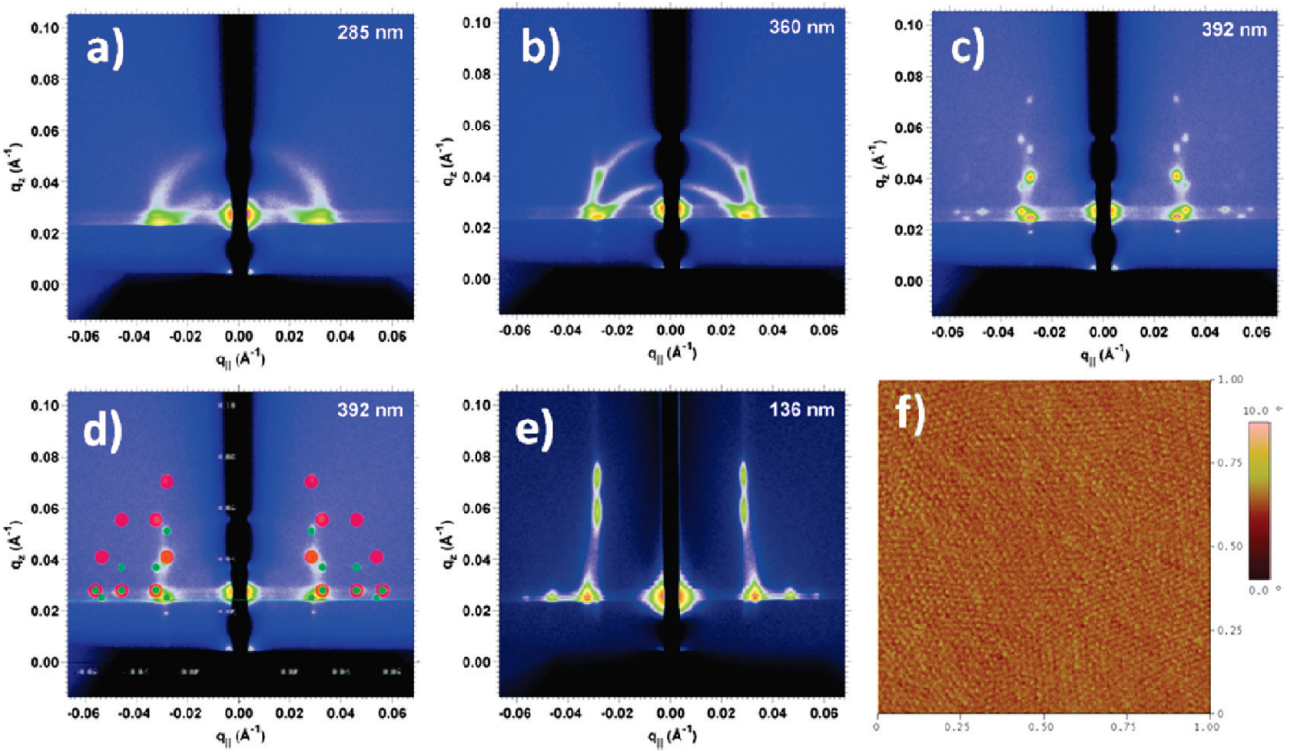

Figure 4. (a−c) In situ swelling of the block copolymer thin film in acetone vapor. Upon swelling to a ratio of 2.47, a change from cylinders to spheres begins. After keeping the film swelled above 360 nm for 1 h, individual peaks can be seen indicating a spherical morphology. (d) Scattering from the swollen, spherical film along with an overlay of the modeled scattering from a stretched BCC lattice. (e) The GISAXS profile of the dried film. Scattering consistent with a FCO spherical morphology is observed. (f) AFM height image after processing in acetone vapor. The height scale is 10 nm.

Table 1. In-Plane Nearest-Neighbor Distances (nm) of the Various Self-Assembled Structures As Obtained by AFM and GISAXS

	standing cylinders as-spun	lying cylinders THF annealed	BCC(110) spheres acetone annealed	BCC(110) spheres THF → acetone annealed	lying cylinders acetone → THF annealed
AFM	18.8 ± 2.4	23.3 ± 2.0	24.2 ± 3.2	25.1 ± 2.7	23.2 ± 1.5
GISAXS	18.6 ± 1.7	22.5 ± 0.8	23.3 ± 1.1	23.5 ± 1.1	22.4 ± 0.9

to a spherical one.[4] Previous ex-situ work confirmed that annealing in acetone resulted in a face-centered orthorhombic spherical structure within the film upon drying. Similar to annealing in THF, a critical swelling ratio was required in acetone annealing before the polymer chains were sufficiently mobile for reordering to occur. For an order−order transition to occur, not only do the chains require adequate mobility to reorganize, but each block must also be swelled to possess the appropriate volume ratio within the polymer phase diagram which is the driving force of the transition.

In situ GISAXS images were once again taken at an incident angle $\alpha_i = 0.16°$, higher than the critical angle of the film (Figure 4). The film thickness of the samples prior to annealing for this experiment was found to be 146 nm (film thickness monitor). Swelling to 392 nm (268% of the original thickness) was needed in order to obtain sufficient chain mobility for self-assembly, larger than the necessary swelling ratio seen from the THF annealing process (218%). This phenomenon may be understood in terms of the solvent selectivity for the two blocks. In order for the block copolymer to have sufficient mobility to self-assemble via solvent vapor annealing, both blocks must be sufficiently swollen such that the glass transition temperature (T_g) of the block drops below the annealing temperature (here, room temperature).[37] An extension to the Dimarzio et al. thermodynamic model explaining the glass transition temperature depression due to a diluent was done by Chow.[38,39] He showed for small molecule solvents the size and concentration of the diluents were the main determinants affecting the drop in the glass transition temperature. Further evidence for the glass temperature depression under solvent vapor uptake and its role in block copolymer thin film kinetics was recently provided be Di et al.[40]

The T_g of PHOST was measured to be 180−190 °C,[4] and while the T_g of PαMS is difficult to measure due to its thermal degradation, the value is known to be ~170 °C[41]—hence both values are significantly higher than room temperature. In the case of the nonselective THF solvent, even swelling of both blocks leads to their plasticization with minimal swelling. Acetone, however, would be expected to swell the PHOST block far beyond the value needed for plasticization, before the PαMS block swells sufficiently for its T_g to be suppressed below room temperature. Alongside with the mobility increase, a sufficiently high PHOST volume fraction must be achieved that acts as the driving force for the phase transition.

At the start of the swelling process, the Bragg rods, once again, disappear (not shown). However, rings appear at a thickness of 285 nm, indicating the formation of a phase-separated morphology, though one lacking directional orientation (Figure 4a). As the swelling ratio is taken above what is necessary for reordering to occur in THF vapors, the polymer can be sufficiently plasticized to start reorganizing. The film thickness was slowly raised until additional changes were seen to occur in the scattered GISAXS images. Individual peaks replaced the ring structure, beginning when the film

is 360 nm thick (Figure 4b), and the individual peaks obtain maximum intensity when the film thickness is 392 nm (Figure 4c). The films were held at this value for 60 min, and no further changes were observed.

Our results indicate that holding the film over time at the same swelling ratio does not lead to changes in morphology; instead, the morphology was found to change at very precise swelling ratios and that the morphology changes are spontaneous once these swelling ratios are achieved. Also worth noting is that no ordered cylindrical morphology is observed in the GISAXS images before scattering from the formation of ordered spheres appears. This indicates that the block copolymer swells unevenly enough to direct a transition to a spherical morphology before sufficient swelling for mobility is achieved. Note that the spherical phase reflections are not smeared out into arcs; hence, the spherical phase is highly oriented with respect to the substrate.

Interestingly, the scattered peaks in the swollen film cannot be modeled by scattering from a BCC lattice. The model only fits when a BCC lattice is stretched in the z direction by 6%, indicating a face-centered orthorhombic (FCO) morphology. We attribute the stretched lattice to the film being freely swollen along the surface normal, whereas swelling in the lateral direction is restricted. The spheres are able to rearrange in the z direction to accommodate the swelling, while being unable to fully rearrange in the lateral direction, resulting in a stretched BCC lattice. Figure 4d shows the theoretical scattered peaks from a stretched BCC lattice mapped on top of the actual scattered peaks, which appear to be in agreement. The red dots signify upward splitting, while the green dots signify downward splitting attributed to refraction/reflection effects associated with the DWBA scattering theory.[36,42] An orthorhombic morphology was observed by Stein et al. in block copolymer films possessing spherical morphology for various film thicknesses, between 4 and 23 layers, as obtained by spin-coating and thermal annealing.[43] In our system, we found the vertical distance between the spherical layers to be 20.3 nm with a film thickness of 392 nm, or about 19 layers of spheres. To our knowledge, this is the first observation of this thin film packing behavior in solvent annealed films.

Upon fast drying of the film, the scattering images show that the stretched FCO geometry of the spheres in the fully swollen film appears to change to a compressed, rather than elongated, FCO geometry (Figure 4e). The compression from the drying process in the z direction causes the unit cell to shrink in the same direction, causing the FCO lattice to be compressed compared to the BCC bulk phase. The elongation of the off-specular peaks is further evidence of solvent evaporation. Ideally, spheres would produce scattered peaks which are symmetric in shape; however, the peaks seen from the dried films are elongated along q_z, suggesting a compression of the spheres in the direction normal to the film surface.

The AFM images in Figure 4f show the surface morphology after annealing in acetone vapor. Although dotlike features can be seen when comparing the AFM images between the as-spun and acetone annealed films, we see increased ordering of the dots in Figure 4f. Also, the nearest-neighbor spacing of 24.2 nm calculated from the power spectral density from the AFM image is in fair agreement with the 23.3 nm obtained from modeling the FCO geometry in the scattered images obtained from GISAXS.

Reversible Morphology Switching. Switching the morphology between spherical and cylindrical morphology is possible via alternating solvent annealing sessions with THF and acetone.[4,21] Hence, it is more accurate to talk in terms of *solvent vapor processing* rather than a simple anneal. Here we demonstrate the mechanism of morphology switching in comparison to processing a film without solvent anneal history, showing that morphology formation is independent of solvent anneal history.

A film previously annealed in acetone vapor was placed in the solvent annealing chamber and subjected to THF vapor processing to take the polymer from a FCO spherical morphology to parallel cylinders. To perform the opposite transition, a film preannealed in THF vapor underwent acetone vapor treatment. As before, GISAXS measurements were performed at an angle of incidence above the polymer critical angle, $\alpha_i = 0.16°$, to probe the whole film interior during swelling. The initial thickness of the films were 131 and 144 nm for the preannealed acetone film and preannealed THF film, respectively.

Figure 5 shows the cycle from spherical morphology after acetone treatment to cylindrical morphology after annealing in THF and back to spherical morphology again. The acetone preannealed film (Figure 5a) was swollen in THF from an initial thickness of 131 to 311 nm (237%) and held above this thickness for 60 min. As observed previously for THF annealing of an as-spun film, scattering from the spheres was seen to begin disappearing within 2 min as the film rapidly swelled to 168 nm thickness (not shown). Upon further swelling, a single pair of peaks appear on the Yoneda band consistent with the spacing of the parallel cylindrical morphology and in contrast to the two sets of peaks visible in the as-spun film annealed in THF (Figure 5b).

Peaks consistent with the initial spherical morphology never reappeared—this was expected as the kinetically trapped (metastable) spherical morphology can now relax back toward the thermodynamically stable cylindrical morphology expected from the block volume fraction of the polymer. Upon reaching a thickness of 311 nm, peaks consistent with a parallel cylinder formation emerge, accompanied by the typical peak splitting when the angle of incidence is above the critical angle of the film, though below the critical angle of the substrate (Figure 5c). Scattering consistent with parallel cylinders is observed in the film after drying, and the film returns to the same dried-state thickness (Figure 5d). The peak positions are also in agreement with THF vapor processing of an as-spun film.

Annealing a THF preannealed film (Figure 5e) in acetone vapors reveals a subtly different behavior. Instead of the scattered peaks from the parallel cylinders disappearing in the initial couple minutes of rapid swelling, as in the case of the as-spun film, rings slowly appear, suggesting the emergence of randomly oriented cylinders. The absence of a sudden transition is not unreasonable, as the cylindrical morphology is stable for this particular block copolymer sample. When the film swelled to 370 nm (257%), additional scattered peaks started appearing while the rings became more faint. The film thickness was sustained above 370 nm for about 1 h. As seen previously in the as-spun film annealed in acetone, peaks consistent with an FCO lattice appear in the swollen state, corresponding to a BCC lattice stretched in the direction perpendicular to the film plane. Upon drying the film, the observed GISAXS image reveals FCO spheres indicating, again, vertical shrinkage of the film during drying.

The peak positions for the double solvent processed films are in good agreement with the initial structures obtained by vapor processing as-spun films. Comparison of the nearest-neighbor (NN) spacings of the self-assembled structures between the solvent processed films is shown in Table 1. The relation between NN distances of lying cylinders and

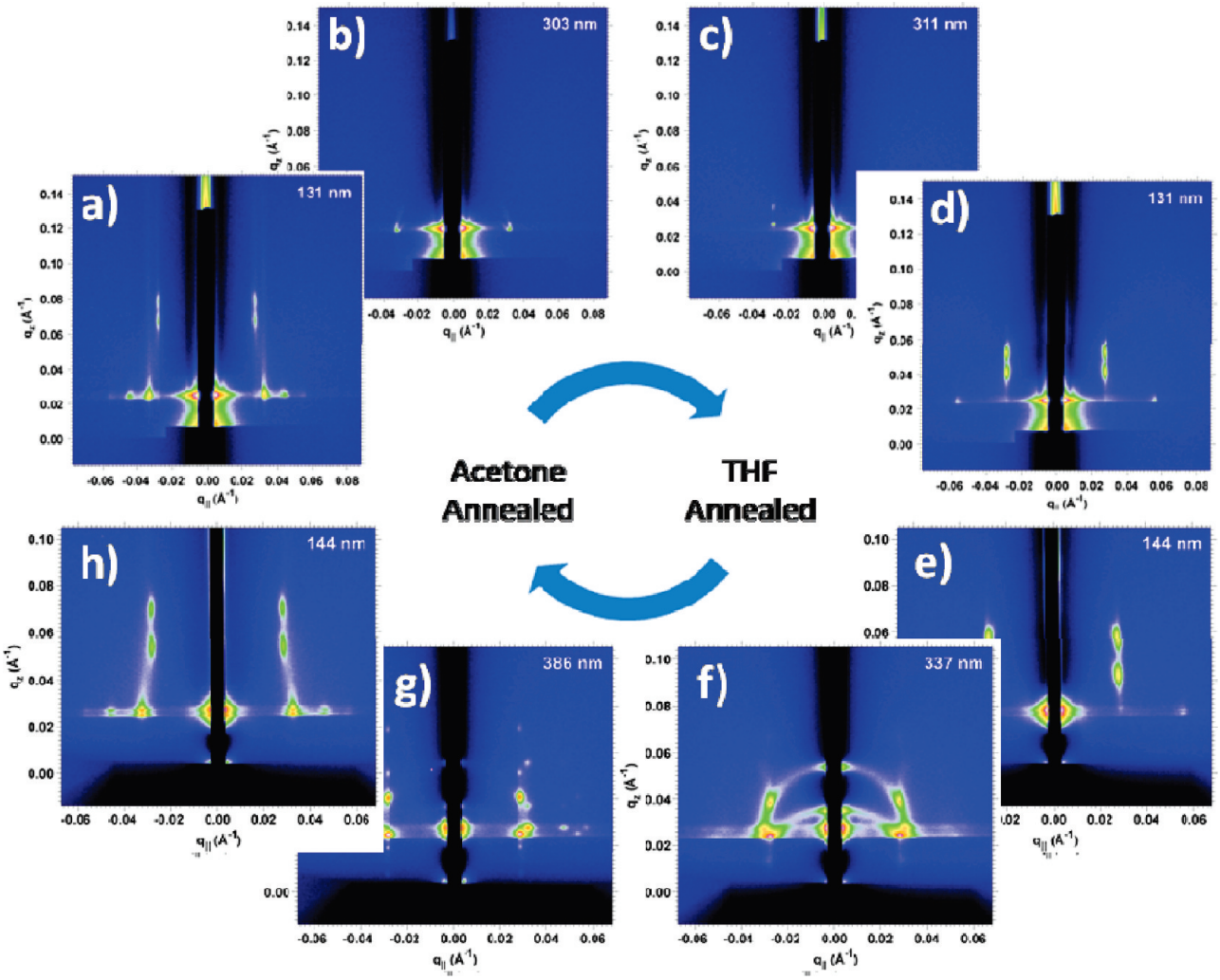

Figure 5. Reversible morphology control through solvent processing as probed in situ and in real time with GISAXS. Thin films with spherical morphology obtained through acetone vapor treatment are shown to transition to parallel cylinders upon THF vapor annealing and returned to a spherical morphology upon successive exposure to acetone vapor.

BCC (110) spheres is in good agreement with a classic study of the bulk morphology by Hashimoto and co-workers.[44] They studied the thermoreversible morphological transition between cylinders and spheres of polystyrene-*block*-polyisoprene. In their observations, they noticed that the (110) *d*-spacing of BCC spheres lattice, d_{110}^{BCC}, was equal to the (100) *d*-spacing of the hexagonal cylinders lattice, d_{100}^{HEX}. Relating the hexagonal and BCC nearest-neighbor distances to the *d*-spacings results in $d_{NN}^{BCC} = 1.061\ d_{NN}^{HEX}$.

Comparing the lateral NN spacings of our annealed films to the results of Hashimoto's work, we see that they are compatible with each other and that $d_{110}^{BCC} = d_{100}^{HEX}$ holds for our samples as well. In addition, we analyzed the associated AFM images of the films and again arrived at the same conclusion. Hence, the phase change in our vapor-processed films must have followed a similar mechanism as determined for the thermal cycling in the bulk study.

Conclusion

Solvent vapor treatment is a powerful processing technique that enables direct control over the morphology and ordering within block copolymer thin films. Not only have we demonstrated with PαMS-*b*-PHOST the ability to direct the morphology of self-assembled domains to hexagonally packed cylinders or FCO spheres, but we have shown that the process is completely reversible. Moreover, the ability to anneal films on a faster time scale than conventionally needed for thermal annealing offers an additional advantage for solvent annealing.

In order to exploit the benefits of solvent annealing completely, the mechanism must be fully understood. We have shown for the annealing process to take effect the polymer must be swollen sufficiently for ordering to occur—the polymer must be plasticized sufficiently for the polymer chains to be mobile enough to reorganize at room temperature. For the order−order transition to occur, the additional variable of solvent selectivity enables tuning of the block volume fraction, and thus the morphologies formed. In the response of an acetone annealed film to THF annealing, the quick relaxation away from the kinetically trapped spherical morphology was observed in contrast to the as-spun annealed films. Morphology of films annealed in both acetone and THF from directly spin-coated films are indistinguishable from films solvent processed previously. Evaporation of the solvent results in compression of the film thickness, but the morphology is otherwise maintained in the dried films.

Acknowledgment. This work was supported by the National Science Foundation Materials World Network (Award DMR 0602821), the NSF NIRT (Award CTS 0304159), and the Semiconductor Research Consortium. M.Y.P. was supported by the National Science Foundation (Award DMR 0518785),

and J.K.B. was supported by fellowships from Motorola and IBM. E.L.S. appreciates support by the Semiconductor Research Corporation. This work was performed using facilities at the Cornell High Energy Synchrotron Source (CHESS), the Cornell Center for Materials Research (CCMR), and The Cornell Nano-Scale Facility (CNF). CHESS is supported by the NSF and the National Institutes of Health/National Institute of General Medical Sciences under NSF Award DMR-0225180. CCMR is supported by NSF Award DMR 0520404, part of the NSF MRSEC Program. CNF, a member of the National Nanotechnology Infrastructure Network, is supported by NSF Award ECS-0335765.

References and Notes

(1) Segalman, R. A. *Mater. Sci. Eng., R* **2005**, *48* (6), 191–226.
(2) Tang, C.; Lennon, E. M.; Fredrickson, G. H.; Kramer, E. J.; Hawker, C. J. *Science* **2008**, *322* (5900), 429–432.
(3) Crossland, E. J. W.; Kamperman, M.; Nedelcu, M.; Ducati, C.; Wiesner, U.; Smilgies, D.-M.; Toombes, G. E. S.; Hillmyer, M. A.; Ludwigs, S.; Steiner, U.; Snaith, H. J. *Nano Lett*., article ASAP.
(4) Bosworth, J. K.; Paik, M. Y.; Ruiz, R.; Schwartz, E. L.; Huang, J. Q.; Ko, A. W.; Smilgies, D.-M.; Black, C. T.; Ober, C. K. *ACS Nano* **2008**, *2* (7), 1396–1402.
(5) Park, S.; Lee, D. H.; Xu, J.; Kim, B.; Hong, S. W.; Jeong, U.; Xu, T.; Russell, T. P. *Science* **2009**, *323* (5917), 1030–1033.
(6) Xue, C.; Meador, M. A. B.; Zhu, L.; Ge, J. J.; Cheng, S. Z. D.; Putthanarat, S.; Eby, R. K.; Khalfan, A.; Bennett, G. D.; Greenbaum, S. G. *Polymer* **2006**, *47*, 6149–6155.
(7) Zhang, R.; Yokoyama, H. *Macromolecules* **2009**, *42*, 3559–3564.
(8) Li, M.; Douki, K.; Goto, K.; Li, X.; Coenjarts, C.; Smilgies, D. M.; Ober, C. K. *Chem. Mater.* **2004**, *16* (20), 3800–3808.
(9) Lee, B.; Yoon, J.; Oh, W.; Hwang, Y.; Heo, K.; Jin, K. S.; Kim, J.; Kim, K.-W.; Ree, M. *Macromolecules* **2005**, *38* (8), 3395–3405.
(10) Braga, D.; Horowitz, G. *Adv. Mater.* **2009**, *21*, 1473–1486.
(11) Iovu, M. C.; Zhang, R.; Cooper, J. R.; Smilgies, D. M.; Javier, A. E.; Sheina, E. E.; Kowalewski, T.; McCullough, R. D. *Macromol. Rapid Commun.* **2007**, *28* (17), 1816–1824.
(12) Bates, F. S.; Fredrickson, G. H. *Phys. Today* **1999**, *52* (2), 32–38.
(13) Cochran, E. W.; Garcia-Cervera, C. J.; Fredrickson, G. H. *Macromolecules* **2006**, *39*, 2449–2451.
(14) Okumura, A.; Nishikawa, Y.; Hashimoto, T. *Polymer* **2006**, *47*, 7805–7812.
(15) Olszowka, V.; Hund, M.; Kuntermann, V.; Scherdel, S.; Tsarkova, L.; Boker, A. *ACS Nano* **2009**, *3* (5), 1091–1096.
(16) Kim, S. H.; Misner, M. J.; Xu, T.; Kimura, M.; Russell, T. P. *Adv. Mater.* **2004**, *16* (3), 226–231.
(17) Kim, T. H.; Hwang, J.; Hwang, W. S.; Huh, J.; Kim, H.-C.; Kim, S. H.; Hong, J. M.; Thomas, E. L.; Park, C. *Adv. Mater.* **2008**, *20* (3), 522–527.
(18) Cavicchi, K. A.; Berthiaume, K. J.; Russell, T. P. *Polymer* **2005**, *46*, 11635–11639.
(19) Peng, J.; Kim, D. H.; Knoll, W.; Xuan, Y.; Li, B.; Han, Y. *J. Chem. Phys.* **2006**, *125*, 064702.
(20) Kim, T. H.; Huh, J.; Hwang, J.; Kim, H.-C.; Kim, S. H.; Sohn, B.-H.; Park, C. *Macromolecules* **2009**, *42* (17), 6688–6697.
(21) Bosworth, J. K.; Black, C. T.; Ober, C. K. *ACS Nano* **2009**, *3* (7), 1761–1766.
(22) Smilgies, D.-M.; Busch, P.; Posselt, D.; Papadakis, C. M. *Synchrotron Radiat. News* **2002**, *15* (5), 35–42.
(23) Xu, T.; Goldbach, J. T.; Misner, M. J.; Kim, S.; Gibaud, A.; Gang, O.; Ocko, B.; Guarini, K. W.; Black, C. T.; Hawker, C. J.; Russell, T. P. *Macromolecules* **2004**, *37* (8), 2972–2977.
(24) Kim, S. H.; Misner, M. J.; Yang, L.; Gang, O.; Ocko, B. M.; Russell, T. P. *Macromolecules* **2006**, *39* (24), 8473–8479.
(25) Papadakis, C. M.; Di, Z.; Posselt, D.; Smilgies, D.-M. *Langmuir* **2008**, *24* (24), 13815–13818.
(26) Smilgies, D.-M.; Li, R.; Di, Z.; Darko, C.; Papadakis, C. M.; Posselt, D. *Mater. Res. Soc. Symp. Proc.* **2009**, *1147*, 1147.
(27) Dourdain, S.; Rezaire, A.; Mehdi, A.; Ocko, B. M.; Gibaud, A. *Phys. B: Condens. Matter* **2005**, *357* (1−2), 180–184.
(28) Du, P.; Li, M.; Douki, K.; Li, X.; Garcia, C. B. W.; Jain, A.; Smilgies, D.-M.; Fetters, L. J.; Gruner, S. M.; Wiesner, U.; Ober, C. K. *Adv. Mater.* **2004**, *16* (12), 953–957.
(29) Brandrup, J.; Immergut, E. H.; Grulke, E. A. *Polymer Handbook*, 4th ed.; Wiley: New York, 1999.
(30) Kim, G.; Libera, M. *Macromolecules* **1998**, *31* (8), 2569–2577.
(31) Anastasiadis, S. H.; Russell, T. P.; Satija, S. K.; Majkrzak, C. F. *Phys. Rev. Lett.* **1989**, *62* (16), 1852.
(32) Busch, P.; Posselt, D.; Smilgies, D. M.; Rauscher, M.; Papadakis, C. M. *Macromolecules* **2007**, *40* (3), 630–640.
(33) Busch, P.; Rauscher, M.; Smilgies, D.-M.; Posselt, D.; Papadakis, C. M. *J. Appl. Crystallogr.* **2006**, *39* (3), 433–442.
(34) Martinelli, E.; Menghetti, S.; Galli, G.; Glisenti, A.; Krishnan, S.; Paik, M. Y.; Ober, C. K.; Smilgies, D.-M.; Fischer, D. A. *J. Polym. Sci., Part A: Polym. Chem.* **2009**, *47* (1), 267–284.
(35) Wan, L.; Yang, X. *Langmuir* **2009**, *25* (21), 12408–12413.
(36) Lee, B.; Park, I.; Yoon, J.; Park, S.; Kim, J.; Kim, K.-W.; Chang, T.; Ree, M. *Macromolecules* **2006**, *38*, 4311–4323.
(37) van Krevelan, D. W.; Hoftyzer, P. J. *Properties of Polymers: Their Estimation and Correlation Length with Chemical Structure*, 2nd ed.; Elsevier Scientific Publishing Co.: New York, 1976.
(38) Dimarzio, E. A.; Gibbs, J. H. *J. Polym. Sci., Part A* **1963**, *1* (4), 1417–1428.
(39) Chow, T. S. *Macromolecules* **1980**, *13* (2), 362–364.
(40) Di, Z.; Posselt, D.; Smilgies, D.-M.; Papadakis, C. M. *Macromolecules* **2009**, *43* (1), 418–427.
(41) Huang, D.; Simon, S. L.; McKenna, G. B. *J. Chem. Phys.* **2003**, *119* (7), 3590–3593.
(42) Busch, P.; Rauscher, M.; Smilgies, D.-M.; Posselt, D.; Papadakis, C. M. *J. Appl. Crystallogr.* **2006**, *39* (3), 433–442.
(43) Stein, G. E.; Kramer, E. J.; Li, X.; Wang, J. *Macromolecules* **2007**, *40* (7), 2453–2460.
(44) Sakurai, S.; Hashimoto, T.; Fetters, L. J. *Macromolecules* **1996**, *29*, 740–747.